Journal of Modern Optics

ISSN: 0950-0340 (Print) 1362-3044 (Online) Journal homepage: https://www.tandfonline.com/loi/tmop20

A time-dependent switching anisotropic diffusion model for denoising and deblurring images

P. Jidesh & Santhosh George

To cite this article: P. Jidesh & Santhosh George (2012) A time-dependent switching anisotropic diffusion model for denoising and deblurring images, Journal of Modern Optics, 59:2, 140-156, DOI: 10.1080/09500340.2011.633713

To link to this article: https://doi.org/10.1080/09500340.2011.633713

Published online: 15 Nov 2011.

Submit your article to this journal

Article views: 186

View related articles

Citing articles: 1 View citing articles

Full Terms & Conditions of access and use can be found at
https://www.tandfonline.com/action/journalInformation?journalCode=tmop20

Journal of Modern Optics
Vol. 59, No. 2, 20 January 2012, 140–156

Taylor & Francis
Taylor & Francis Group

A time-dependent switching anisotropic diffusion model for denoising and deblurring images

P. Jidesh* and Santhosh George

Department of Mathematical and Computational Sciences, National Institute of Technology, Karnataka, Srinivasanagar, Mangalore, Karnataka-575025, India

(*Received 9 August 2011; final version received 7 October 2011*)

A conditionally anisotropic diffusion based deblurring and denoising filter is introduced in this paper. This is a time-dependent curvature based model and the steady state can be attained at a faster rate, using the explicit time-marching scheme. The filter switches between isotropic and anisotropic diffusion depending on the local image features. The switching of the filter is controlled by a binary function, which returns either zero or one, based on the underlying local image gradient features. The parameters in the proposed filter can be fine-tuned to get the desired output image. The filter is applied to various kinds of input test images and the response is analyzed. The filter is found to be effective in the reconstruction of partially textured, textured, constant-intensity and color images, as is evident from the results provided.

Keywords: image restoration and enhancement; isotropic/anisotropic switching filter; explicit time-marching

1. Introduction

Image enhancement plays a major role in the present-day image-processing world. It is widely known that images deteriorate during transmission and acquisition [1]. The deterioration of images is generally due to two different phenomena [1]. The first one relates to image acquisition and is mainly due to imaging system artifacts, the best example of which is out-of-focus blur or optical blur, caused by the deviation of an imaging plane from the focus of an optical lens. This phenomenon is rather deterministic in nature. The second one is due to the noise added to the signals and this is rather stochastic in nature. Knowledge about the noise is limited to the probability distribution. Having said that, the noise is random, and if one analyzes it properly, it can easily be observed that the noise can also be data-dependent. However, in most of the imaging modalities, the noise can be modeled as random and independent of the data. Further, in many practical scenarios, the noise is assumed to follow a Gaussian distribution with mean zero and variance σ^2 (Gaussian white noise).

Many methods have been proposed in the recent literature for deblurring and denoising of images [2, 3]. Joshi et al. [3] make use of a statistical model based on a Bayesian framework to estimate the noise features. With the help of the estimated noise features, they denoise the images. The color priors (with a two-color model) are used for deblurring the images in this method. Yuan et al. [2] proposed a method which finds the deconvolution kernel based on the blur and noisy image pairs, using which they determined the residual image (from the image pairs) and deblurred the images with the information obtained from the residual image. However, this method fails to denoise the images effectively. Even though all these methods provide satisfactory results, in some cases they do not guarantee unique and stable solutions. In most practical applications the deblurring and denoising problems are ill-posed in nature, and hence the uniqueness and stability characteristics of the solutions play a vital role in effective reconstructions.

Partial differential equations (PDEs) and variational methods are widely used for image denoising and deblurring [4–8]. In PDE based methods, the image is evolved with respect to time. The evolution eventually results in a simplification or enhancement of the image features. The variational based methods try to find a minimum of the corresponding energy functional and regularize the fidelity and smoothing terms in the functional, using a regularization parameter [5]. Regularized solutions were also provided for some of the PDE based image simplification and enhancement methods [7, 9]. Peter van Beek et al. [10] proposed a regularization method based on the non-local means (NLM) [11] filter. In this work the authors combine the NLM filter with the deblurring term to reconstruct the images. PDE and variational methods are quite well known for handling ill-posed problems like deblurring and denoising, because the

*Corresponding author. Email: jidesh@nitk.ac.in

ISSN 0950–0340 print/ISSN 1362–3044 online
© 2012 Taylor & Francis
http://dx.doi.org/10.1080/09500340.2011.633713
http://www.tandfonline.com

uniqueness and the stability of the solution can be derived effectively. Further, the PDE formulation is genuinely continuous. Thus, their approximations aim to be independent of the underlying grid and often reveal good rotational invariance.

The commonly used regularization functionals are Tikhonov based [12] and total variation (TV) based [5]. The Tikhonov based functional uses the L^2 norm which penalizes on the image edges. In other-words, L^2 norms do not encourage discontinuities in the solution. Therefore, Tikhonov based methods are not widely used in image processing. The TV based approaches use a TV norm, which allows discontinuities in the solution, and thus helps in retaining the edges in the image, while denoising them. However, the evolution of the PDE associated with the TV regularization functional converges slowly and the convergence heavily depends on the time-step parameter. This drawback of TV was addressed to a considerable extent by Marquiana and Osher [13].

Besides the slow convergence, another major shortcoming of TV based regularization methods is the *stair-case* effect. TV based techniques approximate the homogeneous areas in the image with constant-intensity patches that cause a visual discrepancy called the stair-case effect. Many methods were proposed subsequently in the literature to address the stair-case effect. The majority of these methods rely on the energy functionals with higher-order evolution PDEs [7,8]. However, the higher-order PDEs when used in the evolution equations may result in a smoothed output image (with blurred edges). Another improved method was proposed by Suhua et al. [14] and Chaan et al. [15], in which the authors proposed a regularization functional, which is a convex combination of TV norm and L^2 norm, together with a parameter to select the contribution of each of these norms. This method could address the issue due to the stair-case effect to a considerable extent, by providing a better approximation of the homogeneous areas in the images. However, this method also has a slow convergence rate and the stability of the solution depends sensitively on the time-step parameter of the evolution PDE. Another noticeable issue with TV based and Tikhonov based methods is that even though the energy functional is convex, the Euler–Lagrange equations associated with the energy functional are nonlinear and are generally ill-conditioned.

Many implicit and semi-implicit iterative solutions were proposed in the literature for solving this nonlinear PDE, see [16] and [17]. The implicit solution proposed by Chan et al. [16] uses a primal-dual quadratic method, and the linear semi-implicit method proposed by Vogal and Omen [17] uses a fixed-point iteration method. These methods provide impressive results when used for denoising, but they hardly perform well when used for deblurring and denoising problems. In such cases these methods are highly ill-conditioned and the computational cost is extremely high.

The overheads due to the computational complexity of the TV based methods were addressed by Osher et al. [13], who proposed a model based on the level-set motion and established that the steady state can be reached quickly by the explicit time-marching method. In this model the diffusion term is the mean curvature motion (MCM). The MCM is a purely anisotropic diffusion method, in which the level-lines move with a speed proportional to their mean curvature in the direction normal to the level-curves. Hence, the diffusion takes place along the direction of the level-lines, not across it. This property of the filter is desirable in the regions of the images dominated by edges, finer details and textures, whereas it is rather a liability in the smooth or homogeneous areas. In the homogeneous areas the anisotropic diffusion pretends to form constant-intensity patches resulting in the stair-case effect [8].

All these facts (mentioned above) motivated us to propose a time-dependent curvature based image reconstruction method whose steady state is attained quickly by the explicit time-marching method. The proposed filter denoises anisotropically in the areas dominated by the edges and isotropically on the homogeneous areas. The switching of this filter between anisotropic and isotropic behaviors is based on the local image gradient features. The isotropic diffusion on the homogeneous areas approximates the filter to a ''Laplacian'' filter. One can easily observe that the energy functional associated with the ''Laplacian'' is induced by an L^2 norm. In other words, for the energy functional which induces the L^2 norm, the Euler–Lagrange equation will be a ''Laplacian'' operator. As we have already mentioned, the L^2 norm penalizes on the image edges, but rarely leads to the formation of constant patches which results in the stair-case effect. However, in the areas in the image dominated by the edges and finer details (like textures), the diffusion process will get transformed into an anisotropic process and does not diffuse at all in the direction of the gradient, making the edges intact even after many iterations. The experimental results provided show the capability of the method to reduce the stair-case effect while deblurring and denoising the images.

This paper is organized into five sections. Section 2 explains the background of the regularization methods for image reconstruction. The proposed model and the numerical implementations are described in Section 3.

Section 4 gives a detailed explanation and inferences regarding the results and the experiments conducted. Finally we summarize our conclusions in Section 5.

2. An overview of regularization approaches for image enhancement

An image reconstruction problem can be formulated as:

$$Ku + n = u_0, \tag{1}$$

where u_0 is the observed image, u is the actual image, $K : R^2 \to R^2$ is a linear bounded operator defined in R^2 (real two-dimensional space) and n is the noise. Here we assume the noise to be Gaussian white noise with mean zero and variance σ^2 and further, the noise is assumed to be independent of the data. Here K is a blurring operator, which is typically a Fredholm integral operator of the first kind [18] and is assumed to be known. This operator can be written as:

$$(Ku)(x) = \int_\Omega k(x, x')u(x')\mathrm{d}x', \quad x \in \Omega, \tag{2}$$

where k is defined as:

$$k(x, y) = \frac{1}{4\pi\sigma} e^{-(x^2+y^2)/4\sigma}. \tag{3}$$

Here σ is the spread of the Gaussian kernel and Ω is the area of support of the image. If we impose translational invariance on the kernel k in (3), then it becomes a point spread function (PSF). Therefore, Ku can be written as $k*u$, where "*" denotes a linear convolution operator. Now, the problem is to determine the original image u from the observed blurred and noisy image u_0. The above problem belongs to a class of inverse problems, wherein we have to provide a solution to the actual data from the observed data, with some given prior information. In most practical applications the inverse problems will be ill-posed, in the sense of Hadamard [19].

A better way to deal with such ill-posed problems is to consider a variational formulation of the model (1). The main objective is to estimate u from the statistics of the noise, blur and a priori knowledge of the image features, like the smoothness of the image and the existence of edges. Let us assume a functional $J(u)$, which measures the quality of the image u, i.e. a smaller value of $J(u)$ represents a better image. One can note that, under the above assumption, the problem can be solved as a constrained minimization problem:

$$\min_u J(u) \quad \text{subject to } \|k * u - u_0\|_{L^2}^2 = |\Omega|\sigma^2, \tag{4}$$

since

$$\|k * u - u_0\|_{L^2}^2 = \int_\Omega (k * u - u_0)^2 \,\mathrm{d}x \approx E\left(\int_\Omega n^2 \,\mathrm{d}x\right) = |\Omega|\sigma^2,$$

where $E(x)$ stands for the expectation of the random variable x and k is defined as in (3). Here Ω denotes the image domain and σ^2 is the noise variance.

2.1. Regularization methods

Fourier transform based regularization filters (FFT-REG filter) were used earlier, for deblurring and denoising the images [20], and can be written as:

$$\hat{u}(w) = \frac{\hat{u_0}(w)\hat{k}(w)}{\|\hat{k}(w)\|^2 + \alpha}, \tag{5}$$

where $\hat{x}$ denotes the Fourier transform of the function x, α is a positive regularization parameter, $\|\cdot\|$ denotes the usual Euclidean norm and w denotes a frequency variable. The solution is obtained in the frequency domain. The other symbols in (5) are as in (1). One can observe that the space in which the solution is well-defined is the space of bounded variation (BV space). The BV space allows discontinuities in the function, hence the image gets deblurred but hardly gets denoised. Therefore, the obvious alternative is to use the Sobolev regularization filter (SOB-REG-Filter) [20], which is defined in a space that does not allow discontinuities in the function. The Sobolev filter can be written as:

$$\hat{u}(w) = \frac{\hat{u_0}(w)\hat{k}(w)}{\|\hat{k}(w)\|^2 + \alpha S(w)}, \tag{6}$$

where the notation has the same meaning as in (5), and the term $S(w) = \|w\|^2$ is the Fourier transform of the "Laplacian" of the image function u. This filter denoises the image well but penalizes more on the edge features. Therefore, the filters in (5) and (6) do not provide satisfactory reconstruction results.

Another widely used regularization is Tikhonov regularization [12] or the *penalized least squares* method, which uses the regularization functional $J(u) = |\nabla u|_{L^2}$; thus the restoration problem can be written as:

$$\min \int_\Omega |\nabla u|_{L^2} \,\mathrm{d}x \quad \text{subject to } \frac{1}{2}\left(\int_\Omega (k*u-u_0)^2 \,\mathrm{d}x - |\Omega|\sigma^2\right) = 0. \tag{7}$$

Here $|\cdot|_{L^2}$ denotes the L^2 norm. The "Lagrangian" of (7) is written as:

$$\int_\Omega |\nabla u|^2 \,\mathrm{d}x + \frac{\alpha}{2}\left(\int_\Omega (k * u - u_0)^2 \,\mathrm{d}x - |\Omega|\sigma^2\right). \tag{8}$$

The problem can be reduced to an energy functional minimization problem:

$$J(u) = \frac{\alpha}{2}\left(\int_\Omega (k * u - u_0)^2 \, \mathrm{d}x - |\Omega|\sigma^2\right) + \int_\Omega |\nabla u|^2 \, \mathrm{d}x, \tag{9}$$

where α is the regularization parameter (Lagrange multiplier) and ∇u is the gradient of the image function u. Both the terms in (9) are well defined in the space:

$$W^{1,2}(\Omega) = \{u \in L^2(\Omega); \nabla u \in L^2(\Omega)^2\}. \tag{10}$$

The problem $\inf\{J(u), u \in W^{1,2}\}$ admits a unique solution characterized by the following Euler–Lagrange equation:

$$\frac{\partial u}{\partial t} = \alpha k * (k * u - u_0) - \Delta u = 0, \tag{11}$$

where Δu denotes the ''Laplacian'' of u. This PDE is a boundary value problem with Neumann boundary condition:

$$\frac{\partial u}{\partial \vec{n}} = 0, \tag{12}$$

where $\vec{n}$ is the unit outward normal to the curve and the initial condition:

$$u(x, y, 0) = u_0(x, y), \tag{13}$$

where u_0 is the initial image. The initial condition in (13) and boundary condition in (12) are assumed for all the PDEs throughout this paper. Since the ''Laplacian'' operator is isotropic in nature, the diffusion process will diffuse in all directions with equal speed, which would eventually result in a smoothed output image. Therefore, Tikhonov based regularization is not well suited for images with sharp discontinuities (edges or finer details). Further, it can be easily noticed from the energy functional in (9) that the L^p norm with $p = 2$ removes the noise but penalizes more on the gradients corresponding to the edges. Another easy observation is that, as p decrease from 2 to 1, the edge-preserving capacity of the filter gradually increases, with a maximum value when $p = 1$.

Another improved regularization method was proposed by Rudin et al. [5] (ROF-Model). This method uses a total variational (TV) functional in place of $J(u)$, i.e.

$$J(u) = \mathrm{TV}(u) = \int_\Omega |\nabla u| \, \mathrm{d}x = \int_\Omega \sqrt{u_x^2 + u_y^2} \, \mathrm{d}x. \tag{14}$$

Among all the norms, only the TV norm allows discontinuities and therefore, with the help of the TV norm, one can recover the images without losing the majority of edge features present in the images. The ROF model can be written in energy minimization form, as:

$$\min \int_\Omega |\nabla u|_{\mathrm{TV}} \, \mathrm{d}x \quad \text{subject to } \frac{1}{2}\left(\int_\Omega (k * u - u_0)^2 \, \mathrm{d}x - |\Omega|\sigma^2\right) = 0. \tag{15}$$

Here $|\cdot|_{\mathrm{TV}}$ is the TV norm associated with the image function u. The ''Lagrangian'' of (15) is written as:

$$\int_\Omega |\nabla u| \, \mathrm{d}x + \frac{\alpha}{2}\left(\int_\Omega (k * u - u_0)^2 \, \mathrm{d}x - |\Omega|\sigma^2\right). \tag{16}$$

The energy functional for the ROF model can be written as:

$$J(u) = \frac{\alpha}{2}\left(\int_\Omega (k * u - u_0)^2 \, \mathrm{d}x - |\Omega|\sigma^2\right) + \int_\Omega |\nabla u| \mathrm{d}x. \tag{17}$$

The Euler–Lagrange equation associated with this energy functional can be written as:

$$\frac{\partial u}{\partial t} = \alpha k * (k * u - u_0) - \nabla.\left(\frac{\nabla u}{|\nabla u|}\right). \tag{18}$$

The PDE defined in (18) can be written as:

$$\alpha k * (k * u - u_0) - \nabla.\left(\frac{\nabla u}{|\nabla u}\right) = 0, \tag{19}$$

when the steady state is reached. The PDE obeys the boundary condition (12) and initial condition (13). One can easily find that (19) is degenerate when $1/\nabla u \to 0$. Hence, it is common to perturb the initial value of the TV norm with a small positive quantity β. With the perturbation defined above the TV norm is modified as:

$$\int_\Omega \sqrt{|\nabla u|^2 + \beta} dx, \tag{20}$$

where β is a small positive parameter. Hereafter we denote this perturbed TV norm by: $\int_\Omega |\nabla u|_\beta \, \mathrm{d}x$. The natural choice of the space in which the terms in (17) are well defined is

$$V = \{u \in L^2(\Omega); \nabla u \in L^1(\Omega)^2\}. \tag{21}$$

Many methods have been suggested in the literature to solve the Euler–Lagrange equation in (19); see [16,21]. All these methods belong to the time-dependent approximation of the ill-conditioned Euler–Lagrange equation in (19). Both the approaches in [16,21] are inefficient, because the steady state is reached in a very small time step, when the explicit

scheme is used. The following formulation is due to Rudin et al. [5].

$$\frac{u_t^{n+1} - u_t^n}{\Delta t} = -\lambda k * (k * u_t^n - u_0) + \nabla.\left(\frac{\nabla u^n}{|\nabla u^n|_\beta}\right), \quad (22)$$

with the initial condition (13) and the boundary condition (12). Here λ denotes the regularization parameter. As t increases we obtain the restored versions of the input image. The evolution equation in (22) converges very slowly. The diffusion term in (22) is parabolic and is singular for smaller values of $|\nabla u|$. Hence, it would be beneficial to put a restriction on the time-step parameter in order to ensure the stability of the evolution process. This is described by the Courant–Friedrichs–Levy (CFL) condition which relates the time step Δt to the space step Δx by:

$$\Delta t/\Delta x \leq c|\Delta u|, \quad (23)$$

where $c > 0$.

Marquina and Osher [13], in their MO-based model, relax this CFL condition, in order to avoid the difficulties due to the time-step constraints. Their method is a time-dependent model that accelerates the movement of level-curves of u and regularizes the diffusion term in a nonlinear way. They propose to multiply the Euler–Lagrange equation in (19) by the magnitude of the gradient; the model can be read as:

$$u_t = -|\nabla u|\lambda\, k * (k * u - u_0) + |\nabla u|\nabla.\left(\frac{\nabla u}{|\nabla u|_\beta}\right), \quad (24)$$

with the boundary condition in (12) and the initial condition in (13). One can easily observe in (24) that the diffusion term is purely the mean curvature motion (MCM) [22]. In MCM the level-curves move towards the zeros of $k * u - u_0$, with a speed proportional to their mean curvatures. Therefore, the noise gets diffused at a faster rate and the steady state is attained quickly. The areas where $k * u - u_0$ is zero or in the homogeneous areas, only the anisotropic diffusion (induced by MCM) will be active (the effect of the fidelity term will be zero), whereas, at the non-zero points of $k * u - u_0$, the fidelity term will give a contribution regularized by the magnitude of the gradient. This would eventually retain and sharpen the edges while denoising the images. Analytically it can be shown that this solution procedure approaches the same steady state as in (19).

The anisotropic nature of the MCM forces the filter to diffuse only in the direction tangent to the level-curve, because MCM has a component only along the tangent and the component normal to the curve is zero. This property of MCM is highly desirable in the areas of the image dominated by the high-frequency components (or edges and finer details). However, in the constant-intensity areas MCM will result in forming constant-intensity patches causing the stair-case effect.

3. Proposed model

In this paper we propose to couple the fidelity term in (24) with a diffusion term, which behaves like MCM in the areas of the image dominated by edges and finer details, and like a ''Laplacain'' filter in the homogeneous intensity areas. The proposed model results in enhancement of edges, while removing the noise in an anisotropic manner. The proposed method can be mathematically formulated as:

$$u_t = -\lambda|\nabla u|k * (k * u - u_0) + c\big(\phi_\tau(|\nabla u|_\sigma)u_{\eta\eta} + u_{\xi\xi}\big), \quad (25)$$

where ξ is the direction along the level-curve and η is the direction along the gradient. The function $\phi_\tau(x) = 1$ if $x < \tau$, zero otherwise. $|\nabla u|_\sigma$ is the magnitude of the gradient of the Gaussian convolved version of the image (with the standard deviation σ). The initial condition (13) and boundary condition (12) are assumed for this PDE as well. One can easily observe from (25) that in constant-intensity areas the function $\phi(\cdot)$ will return one and the diffusion term will transform to an ordinary ''Laplacian'' filter ($\nabla^2 u$), which is isotropic. Therefore, the diffusion term is: $u_{\xi\xi} + u_{\eta\eta}$. Note that the term $u_{\xi\xi}$ in (25) denotes MCM. In the regions dominated by edges and finer details, the function $\phi_\tau(x)$ will return the value zero; this causes the filter to behave like a MCM filter. The parameter τ in the function $\phi_\tau(\cdot)$ is a gradient threshold parameter. This parameter provides the necessary input to the filter to switch between isotropic and anisotropic behavior. When the value of τ is kept very low (near to zero), the filter switches to a ''Laplacian'' filter, only in the constant-intensity areas, whereas, when the value of τ is quite high, then some of the edge features having the gradient magnitude value less than τ will get smoothed out. Since the smooth regions need not always be constant-intensity regions, the switching of the filter may not give impressive results, if the value of τ is kept very low. Therefore, one should take due care while selecting the value of τ for obtaining proper results. The parameter λ controls the smoothing and fidelity characteristics of the filter. When λ is very small, then the noise features remain not much affected by the diffusion flow. But when λ is quite large then denoising happens to a considerable extent and the stability of the filter will be greatly affected. Therefore, the parameter λ can be chosen as the maximum value allowed for stability. The selection of the parameter λ is crucial in getting the desired results. The parameter c

determines the magnitude of diffusion. The magnitude of diffusion increases with an increase in the value of c. An analysis of the effect of each parameter on the result of the filter is done in Section 4.3.

The anisotropic diffusion term in (25) will not result in approximating the homogeneous regions with constant patches, which eventually results in the stair-case effect. Since the filter does not have any component in the direction of the gradient (in the high-gradient regions in the image), the high-frequency components like the edges and the finer details are not severely affected by the diffusion flow. The proposed filter can still relax on the CFL condition as in (24). This filter speeds up the level-curves of the image function u and regularizes the parabolic diffusion term in a nonlinear way. The initial condition (13) and the boundary condition (12) are assumed for this PDE as well. This solution is well-posed in the space defined by (21) and the unique minimum exists for the PDE in (25) [23].

3.1. Numerical implementation

We have used an explicit Euler scheme for implementing the diffusion equation in (25). Since the equation contains a hyperbolic diffusion term, we use the *upwind* scheme proposed by Sethian et al. [22]. The usual central difference schemes do not work well with the hyperbolic PDE. In other words, the usual central difference scheme results in numerical instabilities in the case of hyperbolic PDEs. We use the ordinary central difference scheme for rest of the terms in the equation. Using the upwind scheme for solving $|\nabla u|$ in (25), results in the following expression:

$$|\nabla u| = \sqrt{D_x^2 + D_y^2} \tag{26}$$

where $D_x = \text{minmod}(u_x^+(x,y), u_x^-(x,y))$, $D_y = \text{minmod}(u_y^+(x,y), u_y^-(x,y))$ and the "minmod" operator is defined as:

$$\text{minmod}(x,y) = \begin{cases} \min(|x|, |y|) & \text{if } xy > 0\ , \\ 0 & \text{Otherwise.} \end{cases}$$

Here

$$\begin{aligned} u_x^+(x,y) &= u(x+1,y) - u(x,y), \\ u_x^-(x,y) &= u(x,y) - u(x-1,y), \\ u_x(x,y) &= (u_x^+ + u_x^-)/2, \\ u_y^+(x,y) &= u(x,y+1) - u(x,y), \\ u_y^-(x,y) &= u(x,y) - u(x,y-1), \\ u_y(x,y) &= (u_y^+ + u_y^-)/2. \end{aligned} \tag{27}$$

For all the other finite differences in (25), we use the usual central difference schemes. Using the central difference scheme, $u_{\eta\eta}$ is discretized as:

$$\frac{u_{xx}|u_x|^2 + 2u_{xy}u_xu_y + u_{yy}|(u_y)|^2}{1 + |u_x|^2 + |u_y|^2},$$

and $u_{\xi\xi}$ is discretized as:

$$\frac{u_{xx}|u_y|^2 - 2u_{xy}u_xu_y + u_{yy}|u_x|^2}{1 + |u_x|^2 + |u_y|^2}.$$

With the help of above discretizations, we can discretize the PDE in (25). Now, the convolution kernel is a Gaussian kernel as defined in (3) with $\sigma = 0.2$.

4. Results and discussion

We have used standard test images "Lena", "phantom", "mri" and "hibiscus" to test the performance of various methods existing in the literature and the one proposed by us. The images "Lena", "phantom", "mri" and "hibiscus" belong to different classes; "Lena" is a partially textured image with homogeneous intensity regions, "phantom" is a constant-intensity image with different constant-intensity regions, "mri" is a textured image with abundant gray-level variations and "hibiscus" is a vector-valued (color) image. These four test images are chosen to demonstrate the capability of the methods under comparison to handle different kinds of images. Note that the test images are degraded using a blurring kernel with mean zero and standard deviation $\sigma = 10$ and Gaussian white noise (independent of the data), resulting in a noisy image with a signal-to-noise ratio (SNR) of 10 dB. Further, all the test images are normalized in the range [0, 1] in all our experiments. We use three qualitative measures: contrast-to-noise ratio (CNR) [24], Pratt's figure of merit (FOM) [25] and the Mean Structural SIMilarity (MSSIM) index [26] to measure the quality of the filtered images quantitatively. The time-step parameter Δt is evaluated as: $1/(1 + \lambda/\epsilon)$, where λ is the regularization parameter and we have fixed it as 0.06 in our experiments. The parameter ϵ is used to regularize the gradient (to avoid blowing up of the values at the zero-gradient areas), the parameter is fixed as 0.04, and the value of the parameter c in (25) is kept as 1 in all our experiments. However, we have shown the effect of all these parameters on the filtered output by varying their values.

In each experiment, the performance of the proposed filter is compared with that of other filters like: the FFT regularization filter (FFT-REG) [20], the Sobel regularization filter (SOB-REG) [20], the Tikhonov regularization method [12], the TV-regularization model [5] and the model proposed by Marquiana and Osher (MO) [13]. The performance

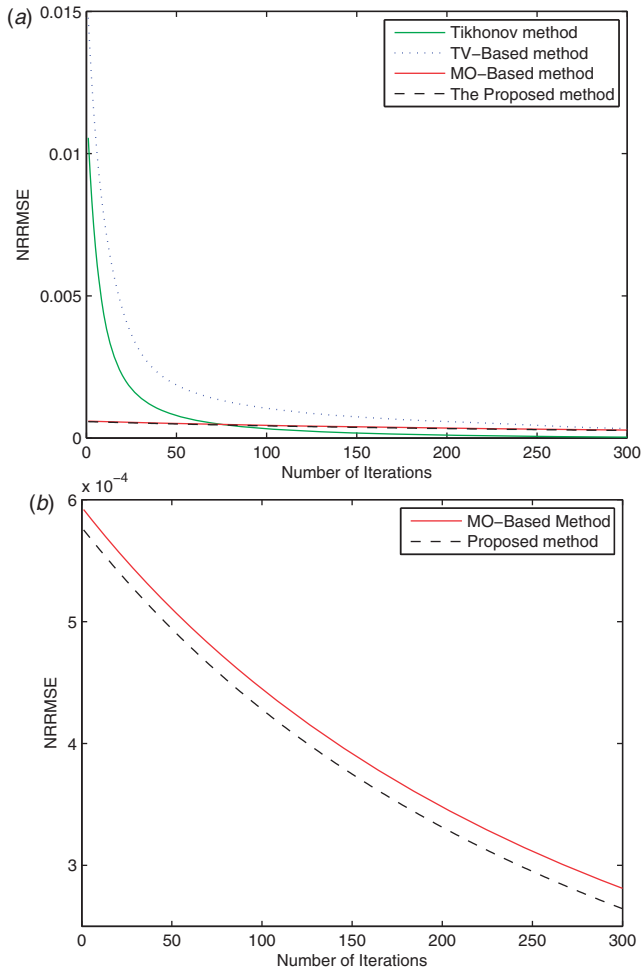

Figure 1. (*a*) NRRMSE plotted for different methods for the image "phantom"; (*b*) NRRMSE plotted for MO-based and the proposed method against the number of iterations. (The color version of this figure is included in the online version of the journal.)

of each method is quantified perceptually (in figures) and quantitatively (in tables and graphs). The results are demonstrated, compared and analyzed in subsequent sections.

4.1. The stopping rule

A number of stopping rules were proposed for determining the optimal number of iterations to get the desired results. Many of them rely on the normalized mean square error in the subsequent iterations or absolute error in each iterations, etc. [5,7,27]. Here we propose to use the normalized relative root mean square error (NRRMSE) in each iteration to put a hold on the iteration process. The root mean square error (RMSE) is defined as:

$$\mathrm{RMSE}^n = \left(\frac{1}{M \times N} \sum_{x=1}^{N} \sum_{y=1}^{M} (u^O(x,y) - u^n(x,y))^2 \right)^{1/2}, \tag{28}$$

where u^O is the original noise-free image and u^n is the image obtained after n iterations using the method under consideration. We define NRRMSE as:

$$\mathrm{NRRMSE} = \inf_n \frac{|\mathrm{RMSE}^n - \mathrm{RMSE}^{n+1}|}{\mathrm{RMSE}^{n+1}}. \tag{29}$$

The NRRMSE keeps on decreasing with each iteration and becomes less than a threshold t after a finite number of iterations. The infimum of the values of n, for which the NRRMSE becomes less than the threshold t, is taken as the optimal iteration number. The reconstruction will be optimal when the iteration number is fixed in this way. The graph in Figure 1 shows the optimal iteration number for different methods existing in the literature and for the method proposed in this paper. In Figure 1(*a*) we plot the NRRMSE of different methods along with the proposed one, for different iteration numbers. In Figure 1(*a*) the variation of NRRMSE against the

Figure 2. Results of various filters applied to the image ''Lena'': (*a*) original figure; (*b*) blur and noisy figure (out of focus blur generated using a Gaussian kernel; SNR of noisy image is 10 dB); (*c*) after applying the FFT-REG filter; (*d*) after applying the SOB-REG filter; (*e*) after applying the Tikhonov method; (*f*) result of applying the TV model; (*g*) result of the MO model; (*h*) result of the proposed model. Row profile of the image ''Lena'' (200th row is selected): the one-dimensional profile of the original, noisy and reconstructed images: (*i*) after applying the FFT-REG filter; (*j*) after applying the SOB-REG filter; (*k*) after applying the Tikhonov method (*l*) result of applying the TV model; (*m*) result of the MO model; (*n*) result of the proposed model. (The color version of this figure is included in the online version of the journal.)

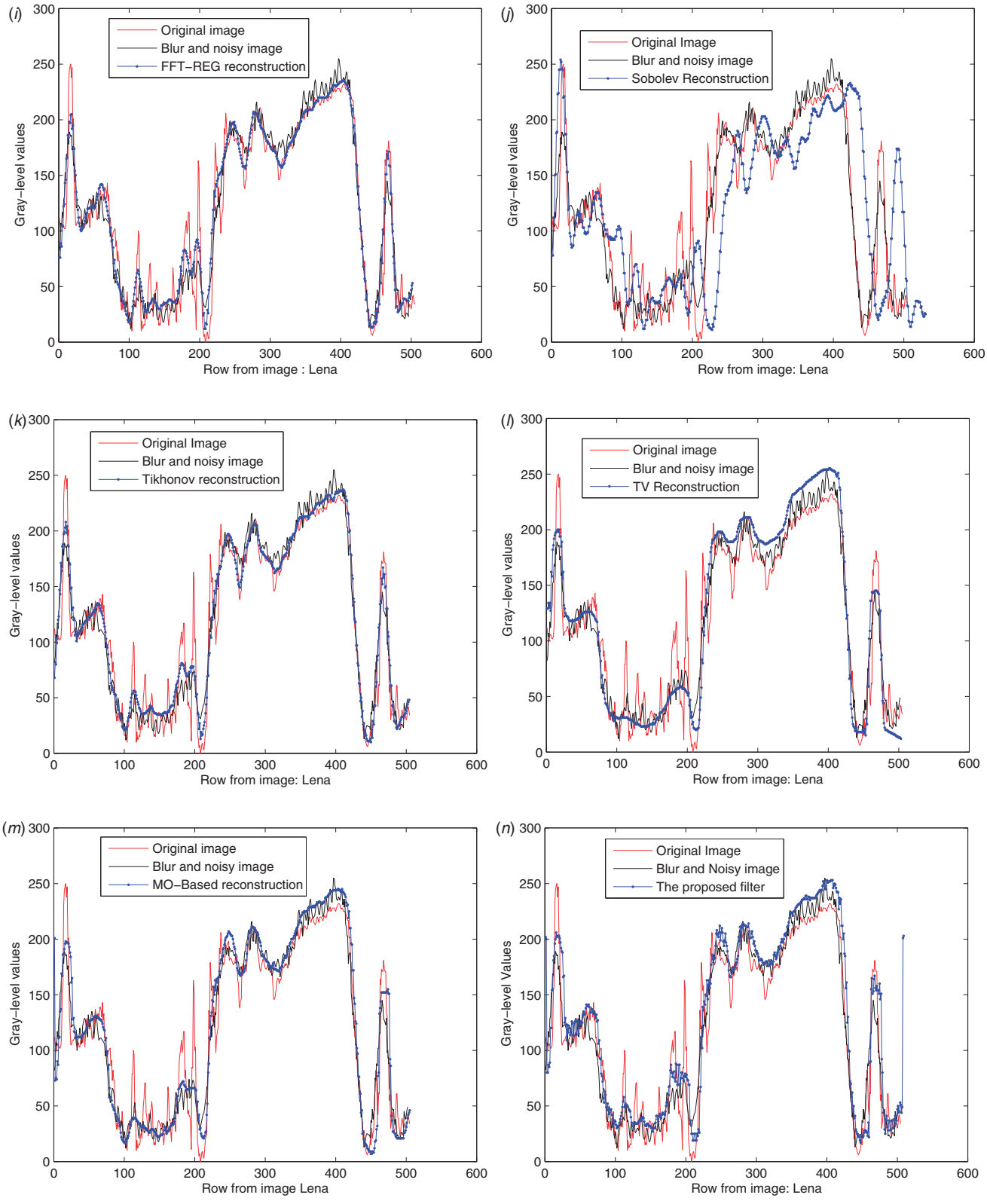

Figure 2. Continued.

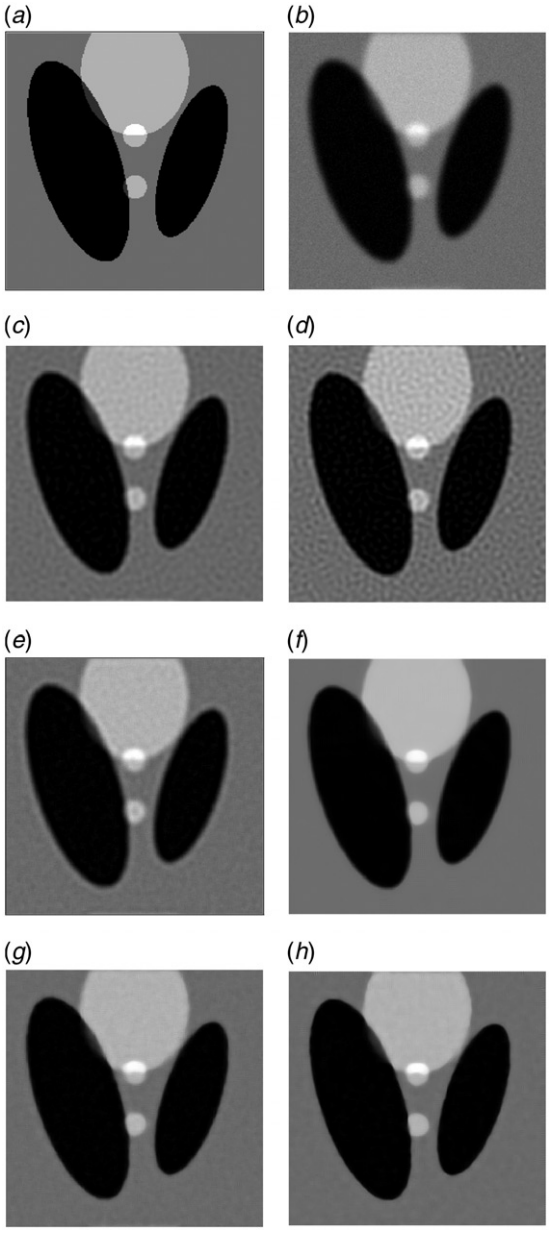

Figure 3. Results of various filters applied to the image "phantom": (*a*) original image; (*b*) blur and noisy image (out of focus blur is generated using a Gaussian kernel; SNR of noisy image is 10 dB); (*c*) after applying the FFT-REG filter; (*d*) after applying the SOB-REG filter; (*e*) after applying the Tikhonov method; (*f*) result of applying the TV model; (*g*) result of the MO model; (*h*) result of the proposed model.

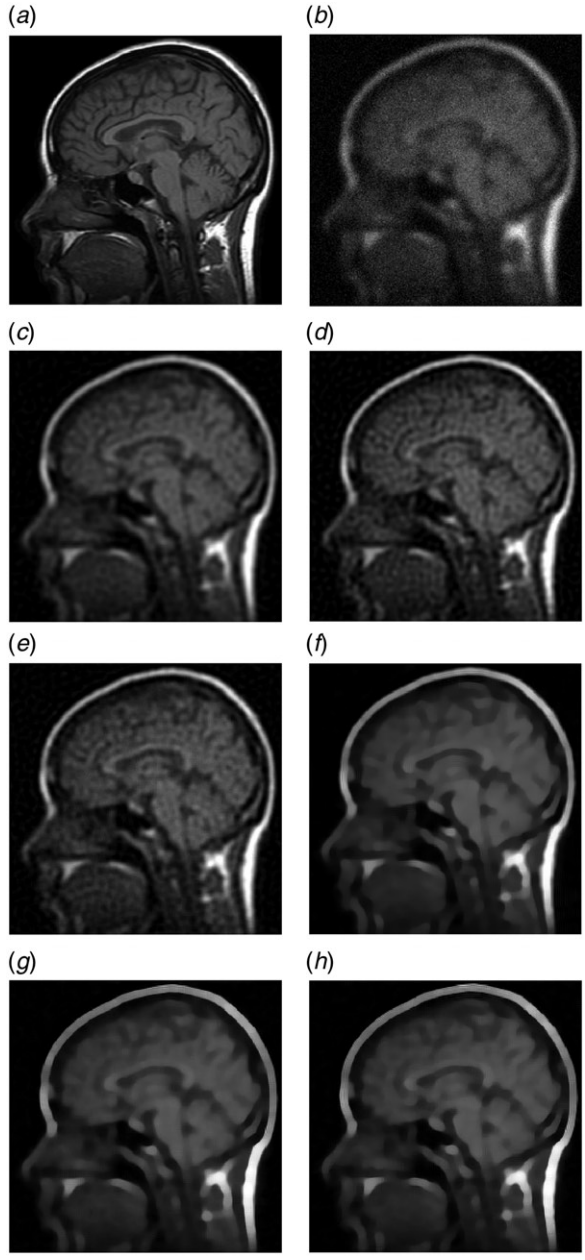

Figure 4. Results of various filters applied to the image "mri": (*a*) original image; (*b*) blur and noisy image (out of focus blur is generated using a Gaussian kernel; SNR of noisy image is 10 dB); (*c*) after applying the FFT-REG Filter; (*d*) after applying the SOB-REG filter; (*e*) after applying the Tikhonov method; (*f*) result of applying the TV model; (*g*) result of the MO model; (*h*) result of the proposed model.

number of iterations is not clearly visible for the MO-based and the proposed methods, so we plot these two methods separately in Figure 1(*b*). The images shown in Figures 2–5 are taken after the corresponding optimal number of iterations for each method. The threshold for calculating the iteration number based on the NRRMSE in (29) is chosen as 0.4×10^{-4} and the value of the parameter σ in (25) is chosen to be 10.

4.2. Quality metrics

There are many statistical methods proposed in the literature to quantify the quality of reconstruction

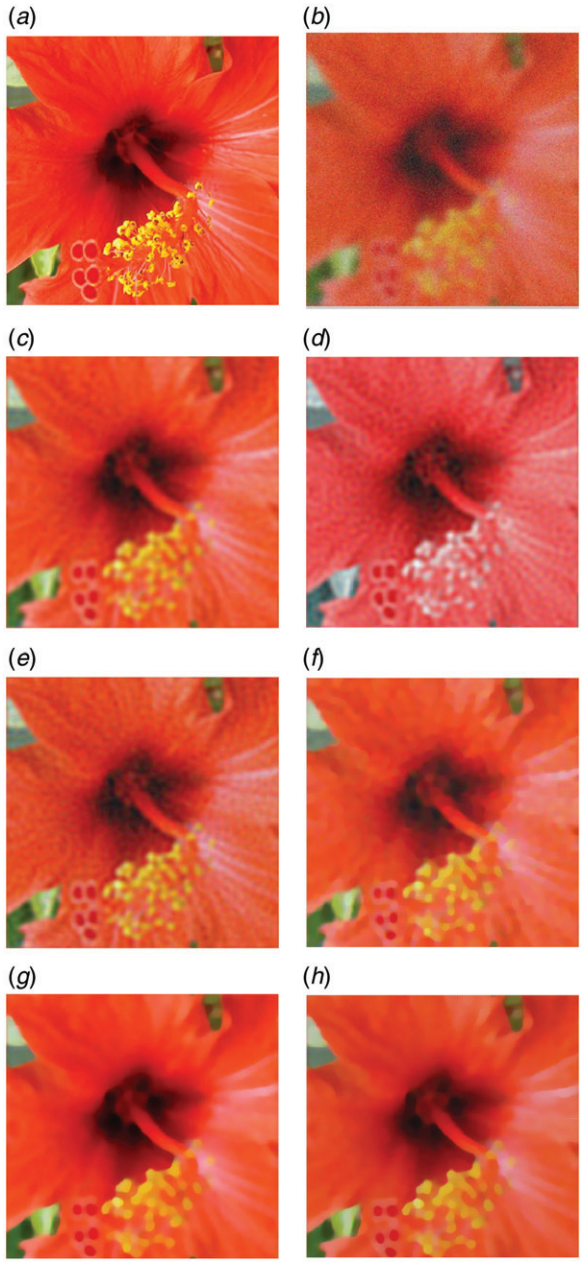

Figure 5. Results of various filters applied to the image "hibiscus": (*a*) original image; (*b*) blur and noisy image (out of focus blur is generated using a Gaussian kernel; SNR of noisy image is 10 dB); (*c*) after applying the FFT-REG filter; (*d*) after applying the SOB-REG filter; (*e*) after applying the Tikhonov method; (*f*) result of applying the TV model; (*g*) result of the MO model; (*h*) result of the proposed model.

methods [24]. One of the most widely used quality measures is the contrast-to-noise ratio (CNR), which measures the contrast enhancing capacity of the filter:

$$\mathrm{CNR} = \frac{\mu_o - \mu_b}{\sqrt{\sigma_b^2 + \sigma_o^2}}, \tag{30}$$

Table 1. The CNR of various methods compared with the proposed one. The SNR of the noisy image is 10 dB.

Images	Noisy	TV	Tikhonov	MO	Proposed
Lena	13.5	12.05	13.6	14.1	16.07
phantom	20.8	33.6	30.7	40.48	66.48
mri	22.1	34.3	29.7	38.9	67.4
boat	20.1	33.8	30.7	41.9	69.4

Table 2. The FOM of various methods compared with the proposed one, for the images corrupted by an SNR 10 dB.

Images	Noisy	TV	Tikhonov	MO	Proposed
Lena	0.503	0.410	0.530	0.492	0.582
phantom	0.516	0.449	0.421	0.5254	0.740
mri	0.546	0.519	0.441	0.614	0.751
boat	0.513	0.499	0.411	0.554	0.810

Table 3. The MMSIM of various methods compared with the proposed one. The SNR of the noisy image is 10 dB.

Images	Noisy	TV	Tikhonov	MO	Proposed
Lena	0.669	0.588	0.658	0.652	0.685
phantom	0.656	0.751	0.647	0.698	0.919
mri	0.666	0.821	0.747	0.798	0.891
boat	0.716	0.751	0.672	0.718	0.909

where μ_o, μ_b are the means of the object and background pixels and σ_o^2, σ_b^2 are the variances of the object and background pixels, respectively. Table 1 shows the CNR values of different methods for the input images "phantom", "Lena', "mri" and "hibiscus".

However, CNR does not reflect the edge, luminance and structure-preserving and enhancing capabilities of the methods. These facts motivate one to use the following quality measures: Pratt's figure of merit (FOM) [25] and the Structural SIMilarity (SSIM) index [26]. These quality metrics (FOM and SSIM), measure the edge and structure preserving capabilities of the method under consideration. The details of these methods are highlighted below.

The performance of various methods in preserving the edges and finer details is compared using Pratt's figure of merit (FOM) [25]:

$$\mathrm{FOM} = \frac{1}{\max\{\hat{N}, N_{\mathrm{ideal}}\}} \sum_{i=1}^{\hat{N}} \frac{1}{1 + d_i^2 \alpha}, \tag{31}$$

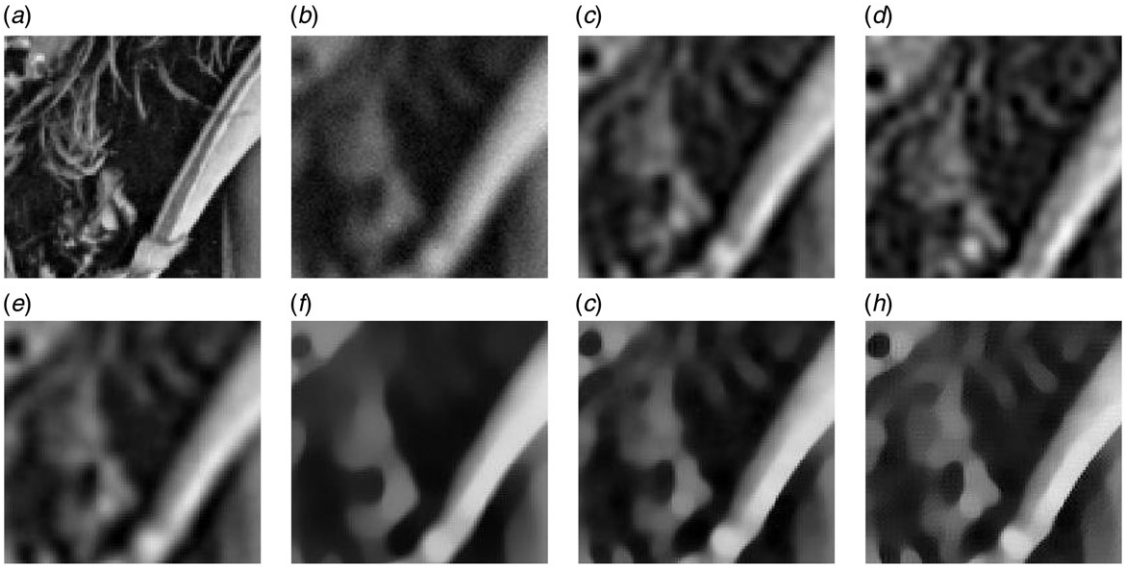

Figure 6. A textured portion of the image ''Lena'' enlarged (for the original and filtered images): (*a*) original image; (*b*) blur and noisy image (out of focus blur generated using a Gaussian kernel; SNR of noisy image is 10 dB); (*c*) after applying the FFT-REG filter; (*d*) after applying the SOB-REG filter; (*e*) after applying the Tikhonov method; (*f*) result of applying the TV model; (*g*) result of the MO model; (*h*) result of the proposed model.

where $\hat{N}$ and N_{ideal} are the number of detected and ideal edge pixels, respectively, d_i is the Euclidean distance between the ith detected edge pixel and the nearest ideal edge pixel and α is a constant typically set to 1/9. FOM ranges between 0 and 1, with unity for ideal edge detection. We apply the Canny edge detector [28] to retrieve the edges in the original and reconstructed images. The standard deviation of the Gaussian kernel in the Canny detector is chosen as $\sigma = 0.1$. Table 2 shows the results of the FOM measure, for different input test images filtered using various methods in the literature and the one proposed in this work.

In addition to the aforementioned methods, we also use the SSIM index to compare the luminance, contrast and structure of two different images [26]. The motivation in using this approach is to find a more direct way to compare the structures of the reference and the distorted signals. This new framework for the design of image quality measures was proposed, based on the assumption that the human visual system is highly adapted to extract structural information from the viewing field. The SSIM is formulated as:

$$\text{SSIM}(x, y) = \frac{(2\mu_x\mu_y + C1) \times (2\sigma_{xy} + C2)}{(\mu_x^2 + \mu_y^2 + C1)(\sigma_x^2 + \sigma_y^2 + C2)}, \quad (32)$$

where x and y denote the content of the local windows in the original and reconstructed images, respectively. The term σ_{xy} denotes the covariance of x and y, and the terms σ_x^2 and σ_y^2 denote the variance of x and y, respectively. Here $C_1 = (k_1 L)^2$ and $C_2 = (k_2 L)^2$, where L is the dynamic range of pixel values and $k_1 = 0.01$, $k_2 = 0.03$ are constants. The measure is applied for non-overlapping windows in both images (original and reconstructed). In this work we measure the mean-SSIM (MSSIM), which is an index to evaluate the overall image quality. It is defined as:

$$\text{MSSIM}(X, Y) = \frac{1}{M}\sum_{j=1}^{M} \text{SSIM}(x_j, y_j), \quad (33)$$

where X and Y are the original and reconstructed images, respectively, x_j and y_j denote the content of the jth local window in the reference and distorted images, respectively, and M is the number of local windows in the image. Table 3 shows the MSSIM tabulated for different test images filtered using various methods in the literature and the one proposed in this paper.

4.3. Analysis and discussion

Figures 2(*a*)–(*h*) and 3 are the output images after applying the different filters in the literature and the one proposed in this paper on the test images ''Lena'' and ''phantom'', respectively. The fact that the proposed method (the image in Figures 2(*h*) and 3(*h*)) well preserves the edges and finer details (while denoising

the image) is quite evident from these images. A textured portion from the image ''Lena'' (after applying various filtering methods) is enlarged and shown in Figure 6 for better visibility. From these enlarged portions, we observe that the capability of the proposed method to retain the finer details and edges is better in comparison to the other methods, whose output is shown in the same figure. We present the response of the proposed method along with the other relevant methods in the literature, when applied to the textured medical image ''mri'' and the color image ''hibiscus'' in Figures 4 and 5, respectively. From these two output images we can arrive at the conclusion that the proposed method can handle textured and color images, the same way it handles the other aforementioned images.

A one-dimensional row profile from the image ''Lena'' is shown in Figures 2(*i*)–(*n*). The 200 th row is captured from the original, noisy and filtered images. This profile gives a clear understanding of the filtering process. We have plotted three row profiles in each graph in Figures 2(*i*)–(*n*). The profiles in each graph correspond to the original image shown as a red continuous line, the blurred and noisy image is shown as the dotted black line and the filtered output is shown as an intermediate dotted blue line. Each graph shown in the figure highlights the output of a specific filtering method. From these graphs, we infer that filtering methods like Tikhonov and Sobolev smooth out the high-frequency components corresponding to the edges and finer details. The Tikhonov and Sobolev filters are defined on a space which does not allow discontinuities in the solutions, and hence the filtered images appear smooth/blurred. However, the noise features are removed effectively by these filters. The other filters, viz. TV, MO and the proposed method are defined on a space which allows discontinuities in the solution. Therefore, these filters retain the edges while denoising the images. Among the methods that allow discontinuities in the solution space, the proposed method well preserves the edges and finer details due to the switching behavior of the filter based on the underlying local gradient features. The demonstration in Figure 2(*n*) substantiates this fact.

For analyzing the quantitative measures like CNR, FOM and SSIM, we have used the test image ''phantom''. The response of the methods for other test images is similar to that of the image ''phantom''. Therefore, the resultant images (filtered output images) are not shown explicitly for other test images. However, these measures are tabulated and shown in the tables, for different images at a specific SNR value. In the same manner, the graph showing the variation of the qualitative measures (CNR, FOM and SSIM) for different noise levels (of input images) are demonstrated only for the image ''phantom''. The results for other test images follow the same pattern as that of the image ''phantom''.

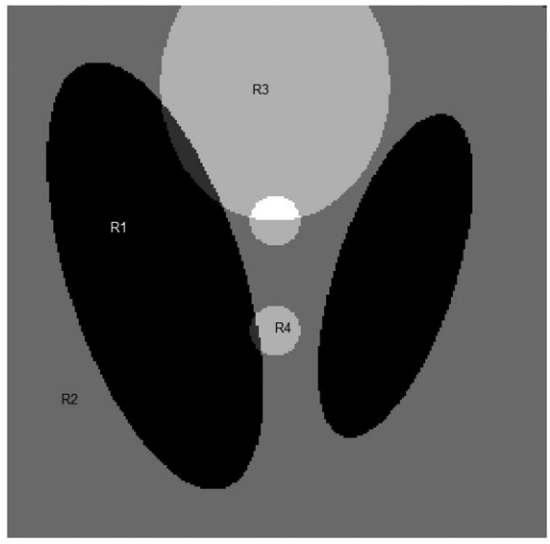

Figure 7. The regions selected for conducting CNR testing.

The CNRs for various methods are tabulated in Table 1. From the table it is quite evident that the proposed method enhances the contrast better compared to the other existing methods. The CNR is calculated for the images after applying the desired filter till the stopping rule (given in Section 4.1) is satisfied. We measured the CNR for the region R1 (in the foreground) taking R2 in the background as shown in Figure 7. Similarly the CNR is measured for the region R3 taking R2 in the background. The graph in Figure 8 shows the variation of CNR for different methods at different noise variances (for the input image ''phantom''). From this graph one can easily see that the proposed method improves the CNR at various levels of noise variances.

Pratt's FOM measures the edge-preserving capability of the methods. As mentioned earlier, a Canny edge detector [28] is used to localize the edges in the original and reconstructed images, respectively. The parameter (variance) of the Canny edge detector is chosen to be 0.1 for our experiments. Table 2 shows the numerical results of Pratt's FOM on the filtered images (and the noisy image), which are filtered using various methods in the literature and the proposed method. The values in Table 2 are in support of the claim that the proposed method preserves and enhances the edges as compared to the other methods in the literature. We plot the variation of the FOM measured under different noise levels (for the input image), for various

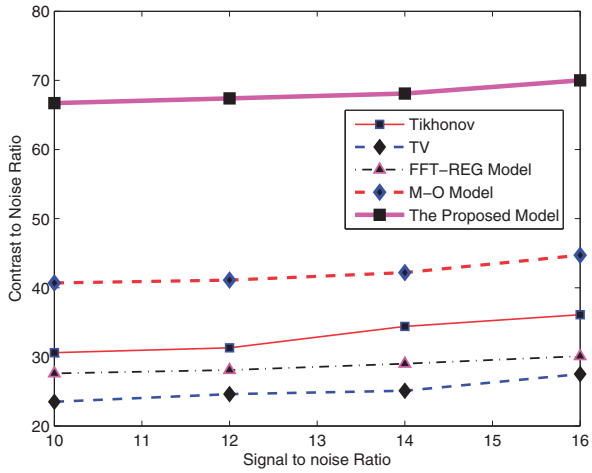

Figure 8. CNR plotted against the SNR for the image "phantom". (The color version of this figure is included in the online version of the journal.)

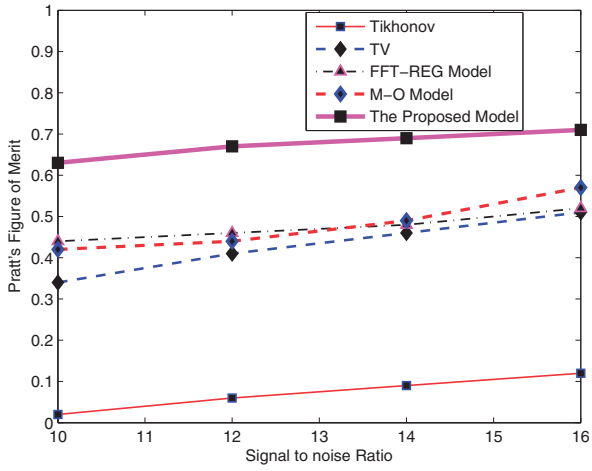

Figure 9. Pratt's FOM plotted against SNR for the image "phantom". (The color version of this figure is included in the online version of the journal.)

methods described in the literature and the proposed method in Figure 9. The graph is quite self-explanatory, regarding the performance of the proposed method. Further, the results of the Canny edge detector on the filtered outputs are shown in Figure 10. The output image after applying the Canny edge detector on the image filtered with the proposed filter is shown in Figure 10(*h*). In this image, one can observe that the edges are preserved and the noise features are removed well, in comparison to the other filters.

The MSSIM shows the structure-preserving capability of the method in hand. The structural similarity index is a key measure to identify the structure-preserving capability of the methods. The SSIM values are tabulated in Table 3 for different input images filtered with various methods in the literature and the proposed method. It is obvious from this table that the proposed method can well preserve the structural details as compared to other methods in the literature. We plot the variation of MSSIM measured under different noise levels for various methods described in the literature and the proposed method in Figure 11. This provides a better analysis of the performance of the proposed method.

The effects of various parameters in the proposed filter in (25) on the filtered images are shown in Figure 12. We have used three parameters to control the magnitude of the diffusion and regularize the filter. The parameter λ controls the magnitude of the diffusion and the fidelity terms. We have shown the output images for three different values of λ,

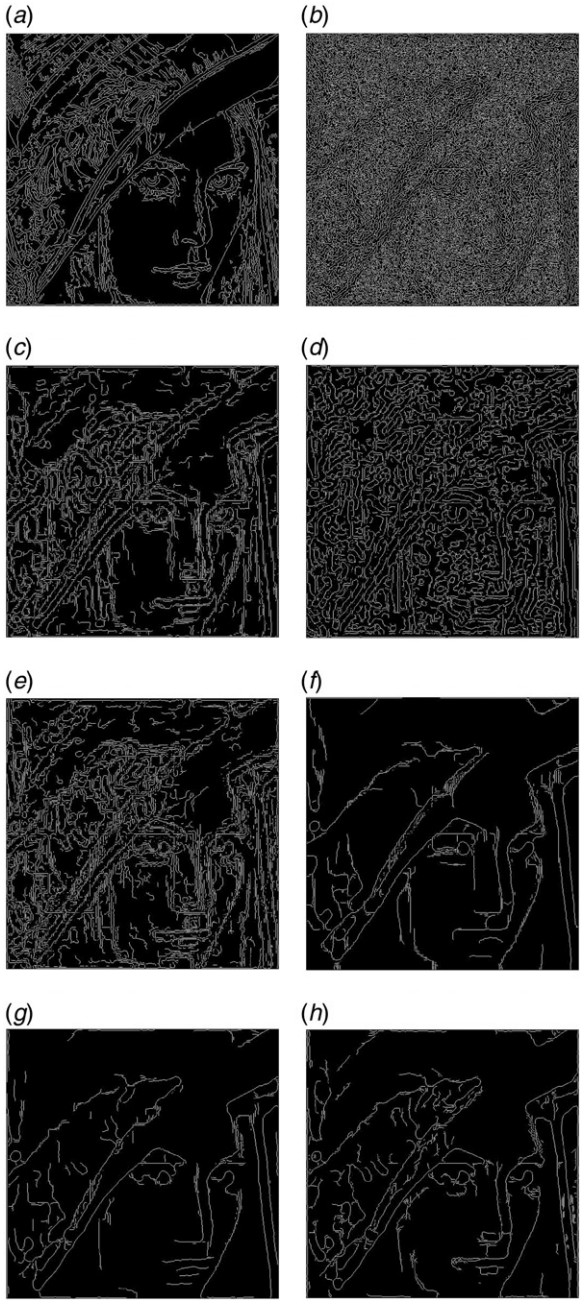

Figure 10. The result of the CANNY edge detector applied to the image "Lena" (filtered using different methods): (*a*) original image; (*b*) blur and noisy image (out of focus blur generated using a Gaussian kernel; SNR of noisy image is 10 dB); (*c*) after applying the FFT-REG filter; (*d*) after applying the SOB-REG filter; (*e*) after applying the Tikhonov method; (*f*) result of applying the TV model; (*g*) result of the MO model; (*h*) result of the proposed model.

i.e. $\lambda = 0.2, 0.06$ and 0.006, in the first row of Figure 12. As the value of λ decreases the effect of the fidelity term is quite evident. In other words, the diffusion keeps on decreasing with a decrease in the value of λ. In the image shown in Figure 12(*c*), the value of λ is chosen to be quite small. Therefore, it is easy to notice that the noise features are not removed properly or the diffusion has not removed the noise in a better scale. When the value of λ is large, the diffusion flow removes the noise, but the numerical instability is highly evident in the results. Hence, λ is chosen to be the maximum value allowed for the stability. The second row of Figure 12 shows the output for various gradient threshold parameters τ. It is evident from these figures that the increase in value of τ causes a better smoothing in the homogeneous image areas. The value of τ determines the switching threshold for the filter. If it is quite high then, for a gradient values less than the threshold value, the filter will act as a "Laplacian" and will smooth out those gradients. We show the result of the filter for three different threshold values ($\tau = 5, 15$ and 25). The effect of the parameter c on the filtered output is shown in the last column of Figure 12. The magnitude of the diffusion is directly proportional to the value of c. The filtered outputs for three different c values (for $c = 0.2, 0.9$ and 1.5) are shown in this row. The figure with $c = 0.2$ is not denoised properly, whereas the output for $c = 1.5$ shows a better denoised image.

5. Conclusions

In this paper we have proposed a time-dependent anisotropic diffusion model for image restoration. The model attains a stable state at a faster rate as compared to other models in the literature. This model diffuses isotropically in the constant-intensity areas and anisotropically in the areas dominated by edges, textures and finer details. The response of the filter is analyzed using different kinds of images having different magnitudes of texture features. The filter is found to enhance the images, with varying magnitude of the texture features. Further, the filter is applied on vector-valued images as well. The results shown in the previous section clearly demonstrate the capacity of the filter to properly enhance textured, partially textured, constant-intensity and color images with utmost attention to the edge and finer details (while denoising them). The behavior of the method is analyzed for different parameters used for fine-tuning the performance of the filter. Under the various conditions mentioned above, the filter is found to behave robustly in reconstructing the images. Finally, the quantitative and qualitative results are in favor of the claim that the proposed method deblurs and denoises the images very well, as compared to the other methods available in the literature.

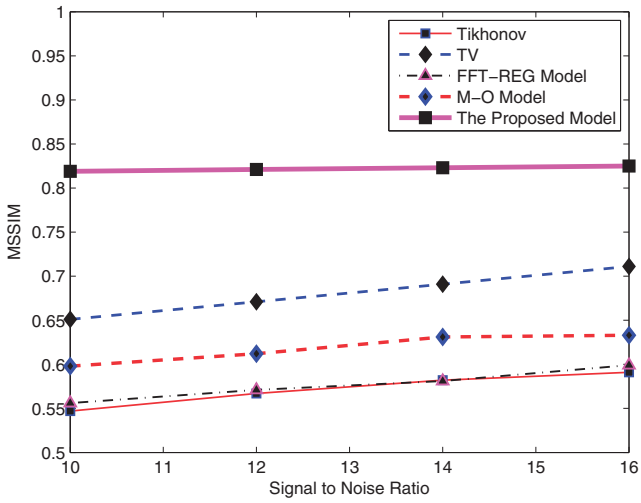

Figure 11. MSSIM plotted against SNR for the image "phantom". (The color version of this figure is included in the online version of the journal.)

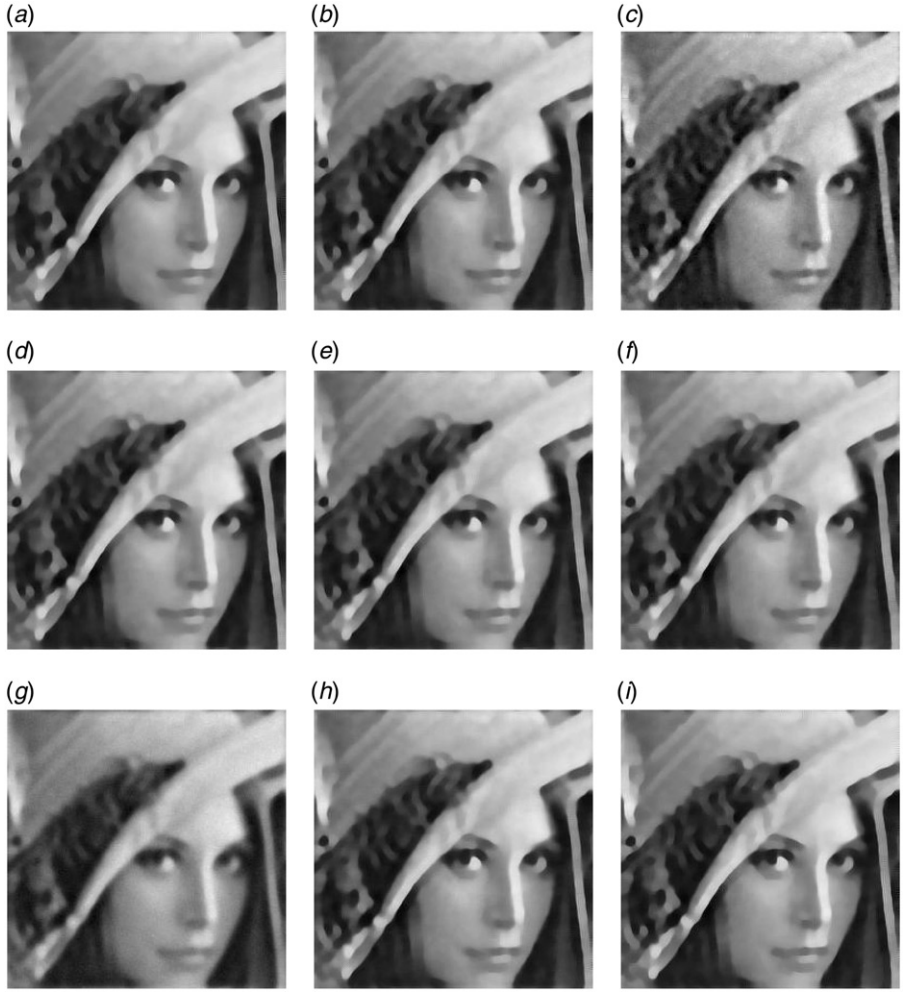

Figure 12. Proposed method applied to the image "Lena" with various values for the parameters. The first row (*a*, *b* and *c*) shows the output images for three different values for the parameter λ in (25) $\lambda = 0.2$, $\lambda = 0.06$, $\lambda = 0.006$, respectively. The second row (*d*, *e* and *f*) shows the output images for three different values for the threshold parameter $\tau = 5$, $\tau = 15$, $\tau = 25$, respectively. The last row (*g*, *h* and *i*) shows the output images for three different values for the parameter $c = 0.2$, $c = 0.9$, $c = 1.5$, respectively.

Acknowledgements

The authors would like to thank the National Institute of Technology, Karnataka, for providing support in carrying out this research work. The authors thank Prof. P. Balasubramani, Mangalore University, India, for his suggestions and help in preparing this manuscript.

References

[1] Aubert, G.; Kornprobst, P. *Mathematical Problems in Image Processing: Partial Differential Equitations and Calculus of Variations*; Springer: New York, 2006.
[2] Yuan, L.; Sun, J.; Quan, L.; Shum, H.Y. *Proc. ACM SIGGRAPH*, 2007, 1–10.
[3] Joshi, N.; Lawrence, C.; Zitnick, R.; Szeliski, D.; Kriegman, J. Image deblurring and denoising using color priors. In *IEEE Conference on Computer Vision and Pattern Recognition*, 2009, 1510–1557.
[4] Kornprobst, P.; Deriche, R.; Aubert, G. Image coupling, restoration and enhancement via PDEs. In *Proceedings of the International Conference on Image Processing*, Vol. 4; IEEE, 1997, pp 458–461.
[5] Leonid, I.R.; Osher, S.; Fatemi, E. *Physica D* **1992,** *60,* 259–268.
[6] Chan, T.F.; Osher, S.; Shen, J. *IEEE Trans. Image Process.* **2001,** *10,* 231–241.
[7] Lysaker, M.; Lundervold, A.; Tai, X. *IEEE Trans. Image Process.* **2003,** *12,* 1579–1589.
[8] You, Y.L.; Kaveh, M. *IEEE Trans. Image Process.* **2000,** *9,* 1723–1730.
[9] Perona, P.; Malik, J. *IEEE Trans. Pattern Anal. Machine Intell.* **1990,** *12,* 629–639.
[10] van Beek, P.; Yang, J.; Yamamoto, S.; Ueda, Y. *Proc. SPIE 7543, 75430R*, 2010, 1–11.
[11] Buades, A.; Coll, B.; Morel, J.M. *SIAM, J. Multiscale Model. Simul.* **2005,** *4,* 490–530.
[12] Tikhonov, A.; Arsenin, V. *Solution of Ill-posed Problems*; John Wiley: New York, 1977.
[13] Marquiana, A.; Osher, S. *SIAM, J. Sci. Comput.* **2000,** *22,* 387–405.
[14] Wei, S.; Xu, H. Stair-casing reduction model applied to total variation based image reconstruction. In *17th European Signal Processing Conference (EUSIPCO 2009)*; EUROSIP; Scotland, 2009, 2579–2583.
[15] Blomgren, P.; Chaan, T.F.; Mulet, P. *Proc. SPIE* **1997,** *3162,* 1964–1977.
[16] Chan, T.F.; Gene H. Golub; Mulet, P. *SIAM. J. Sci. Comput.* **1999,** *20,* 1964–1977.
[17] Vogel, C.; Oman, M. *SIAM, J. Sci. Statist. Comput.* **1996,** *17,* 227–238.
[18] Candella, V.F.; Marquiana, A.; Serna, S. *IEEE Trans. Image Process.* **2003,** *12,* 808–816.
[19] Hardamard, J. *Lecturer on Cauchys Problem in Linear Partial Differential Equations*; Dover: New York, 1953.
[20] Bertero, M.; Boccacci, P. *Introduction to Inverse Problems in Imaging*; IoP Publications: London, 1998.
[21] Chan, T.F.; Mullet, P. *SIAM, J. Sci. Comp.* **1996,** *17,* 227–238.
[22] Osher, S.; Sethian, J.A. *J. Comput. Phys.* **1988,** *79,* 12–49.
[23] Malladi, R.; Sethian, J.A.; Vemuri, B.C. *IEEE Trans. Pattern Anal. Machine Intell.* **1995,** *17,* 158–175.
[24] Gonzalez, R.C.; Woods., R.E. *Digital Image Processing*; Prentice Hall: Upper Saddle River, 2001.
[25] Pratt, W.K. *Digital Image Processing*; John Wiley: New York, 2007.
[26] Wang, Z.; Bovik, A.C. *IEEE Trans. Image Process.* **2004,** *13,* 1–14.
[27] Lee, S.H.; Seo, J.K. *IEEE Trans. Image Process.* **2005,** *14,* 904–909.
[28] Canny, J. *IEEE Trans. Pattern Anal. Machine Intell.* **1986,** *8,* 679–698.